JTTEE5 16:947–953
DOI: 10.1007/s11666-007-9117-5
1059-9630/$19.00 © ASM International

Tribological and Corrosion Behavior of Vacuum Plasma Sprayed Ti-Zr-Ni Quasicrystalline Coatings

Stephan Siegmann, Philippe Kern, Lukas Rohr, and Partha P. Bandyopadhyay

(Submitted March 9, 2007; in revised form June 29, 2007)

This investigation deals with a study of the friction, wear, and corrosion behavior of vacuum plasma sprayed quasicrystalline (QC) $Ti_{41.5}Zr_{41.5}Ni_{17}$ coatings. During pin on disc experiments, a change in the mode of wear has been found to occur with corresponding changes in normal load and sliding velocity. The low thermal conductivity of quasicrystals and its brittleness play a vital role in determining the friction and wear behavior of such materials. When these coatings are subjected to rubbing for a longer period of time, wear occurs by subsurface crack propagation, and subsequent delamination within the coated layer. By comparing the QC to its polycrystalline counterpart during potentiodynamic measurements according to ASTM G 31, higher currents were found over the whole range of potentials for QC when immersed in 1 M HCl solution.

Keywords quasicrystalline (QC) coatings, Ti-Zr-Ni, vacuum plasma spraying, wear and corrosion

1. Introduction

In the year 1984, the discovery of quasicrystal (QC) phases has been reported by Shechtman et al. (Ref 1). It is now known that this material class can offer outstanding material properties, e.g., high hardness (Ref 2, 3), low friction coefficient (Ref 4), low surface energy (Ref 5), high thermo-electric power (Ref 6), etc. Thus, QCs are potential candidates for many industrial applications (Ref 7-9).

Today, many alloys containing a QC phase have been identified also for their potential application in the engineering domain (Ref 10). For example the i-phase of $Ti_{41.5}Zr_{41.5}Ni_{17}$ constitutes are one such system (Ref 11). This phase reportedly is capable of storing hydrogen in large quantities (Ref 12) and hence is a highly potential candidate for fuel cell applications. The i-phase develops in the prior Laves and alpha phase (both HCP) eutectic matrix upon annealing at 570 °C for 7 days (Ref 13). Further annealing at a lower temperature does not cause any transformation of the i-phase. It indicates that the QC phase in question is very stable (Ref 11).

Looking on the corrosion properties of QCs, only a few reports are available today, e.g. (Ref 14-17). Most of them are describing aluminum-based QCs. The corrosion resistance of Al-based QCs is found to depend upon the composition and microstructure of the QC. The addition of chromium to the QC improves its corrosion properties (Ref 14).

QCs in general are not produced by conventional fabrication techniques. They cannot be formed or cast readily. However, alloys having the composition of a QC can be reduced to powder and subsequently can be thermally sprayed to form a coating having the QC phase (Ref 18-22). To date, a few reports are available highlighting the tribological aspects of QC coatings (Ref 7, 8, 10, 21, 23). In general, these studies are limited to Aluminum-based QCs as well. While these materials are expected to yield a high wear resistance and a low coefficient of friction they apparently are somewhat limited by their brittleness (Ref 7). To combat such brittleness, composite QC coatings incorporating a ductile phase as a matrix material have been developed on an experimental basis (Ref 23). The study of friction and wear of QCs are still very much under development and shall be discussed within this article in relation to corrosion properties.

2. Experimental

$Ti_{41.5}Zr_{41.5}Ni_{17}$ powder with a size fraction of $-70+10$ μm has been prepared by gas atomization of the alloy in argon environment. This powder has been vacuum plasma sprayed on stainless steels substrates using a Medicoat 50 kW plasma spraying facility equipped with a six-axis robot.

This article is an invited paper selected from presentations at the 2007 International Thermal Spray Conference and has been expanded from the original presentation. It is simultaneously published in *Global Coating Solutions, Proceedings of the 2007 International Thermal Spray Conference*, Beijing, China, May 14-16, 2007, Basil R. Marple, Margaret M. Hyland, Yuk-Chiu Lau, Chang-Jiu Li, Rogerio S. Lima, and Ghislain Montavon, Ed., ASM International, Materials Park, OH, 2007.

Stephan Siegmann, Philippe Kern, and **Lukas Rohr**, EMPA, Materials Science and Technology, Thun, Switzerland; and **Partha P. Bandyopadhyay**, IIT Kharagpur, Kharagpur, West Bengal, India. Contact e-mail: stephan.siegmann@empa.ch.

Test coupons made of 304 stainless steel with a diameter of 40 mm and thickness 6 mm have been used in these experiments.

The structural analysis of the powders and coatings has been carried out using a Siemens D 5000 X-ray diffractometer with Mo Kα radiation. The XRD data thus obtained has been represented as its Cu Kα equivalent in this article for comparison purpose (Ref 24). The polished and etched cross sections have been subsequently examined under an optical microscope. The porosity of the coatings has been measured by image analysis using the Zeiss KS 400 software. The Vickers hardness of the coatings has been measured using a Leitz Wetzlar hardness tester under a load of 100 g. An average of 10 readings has been reported. The adhesion strength of the coatings has been measured in accordance with the standard EN 582. Before spraying, the substrates have been grit blasted to a surface roughness of $R_a = 5$ μm using white alumina. The parameters used to prepare the set of coatings are listed in Table 1

The friction and wear measurements have been conducted at room temperature, using a CSEM Pin-on-Disc (PoD) tribometer, which permits rotation of a flat specimen against a stationary ball. During the tests, the coefficient of friction (COF) has been monitored continuously. Prior to the tests, the disc samples have been polished to a surface roughness of $R_a = 0.2$ μm. Every trial has been conducted on a fresh track and the specimen has been cleaned ultrasonically in alcohol immediately before the test. The measurement of COF and wear has been done with ZrO_2 balls. The ball diameter was 10 mm. The reported mass loss reflects an average of three readings. The parameters for the ball on disc tests are listed in Table 2. Both the surfaces and polished cross sections of the worn specimens have been observed under a Zeiss DSM 962 Scanning Electron Microscope (SEM) equipped with EDS facilities.

The corrosion resistance of the coatings has been assessed by both immersion corrosion testing following the ASTM G 31 standard and by potentiodynamic measurements (linear sweep voltammetry), respectively. Immersion experiments have been done in a 1 M HCl solution. The corrosion performance of the coating was compared to standard 304 stainless steel. A round area of diameter 12 mm was exposed to corrosive attack for 24 h. The mass of the sample was measured prior to testing using a METTLER AT 261 balance having a resolution of 0.01 mg. After 24 h the specimen was cleaned ultrasonically and the change of mass was recorded. Tests were repeated twice for stainless steel and four times for the coatings.

Potentiodynamic measurements were performed in both 0.5 M HCl + 0.5 M NaCl and 1 M HCl at 28 °C, using an Autolab PGSTAT30 potentiostat working with a three electrode set-up. Discs with 15 mm diameter and about 2.5 mm thickness, consisting of the plasma sprayed coating of about 500 μm thickness (after polishing) on 304 stainless steel substrate, were mounted on a rotating disc electrode set-up and used as working electrode. For comparison, the corrosion behavior of the QC $Ti_{41.5}Zr_{41.5}Ni_{17}$ coating was compared to polycrystalline $Ti_{41.5}Zr_{41.5}Ni_{17}$ (GfE Metalle und Materialien GmbH, Germany) and to commercially pure titanium (grade 2). All samples were mechanically polished with 600 grit paper and ultrasonically cleaned in hexane, acetone, ethanol, and deionized water. In each experiment, a total surface of 1.539 cm^2 was exposed to the electrolyte. A platinum mesh served as counter electrode and a saturated mercury sulfate electrode (SME, Hg/Hg_2SO_4) was chosen as reference electrode. All potentials are given with respect to this electrode. Before linear sweep experiments, the working electrodes were prepolarized at −1.2 V during 60 s for additional in-situ cleaning due to the hydrogen evolution at this cathodic potential.

Table 1 Parameters for vacuum plasma spraying

Parameters	Units	Values
Chamber pressure	mbar	120
Stand-off distance	mm	400
Primary gas flow rate (Ar)	sl/min	50
Secondary gas flow rate (He)	sl/min	10
Arc current	amp	700
Nozzle diameter	mm	6
Powder carrier gas flow rate (Ar)	sl/min	1.3

Table 2 Parameters for PoD tests

Parameters	Values
Ball material	ZrO_2
Normal loads, N	5, 10, 20, 25, 30
Sliding velocities, m/s	0.1, 0.2, 0.4, 0.6, 0.8, and 1.0

3. Results

3.1 Coating Microstructures and Phases

This aspect has been treated in detail in another paper (Ref 25). Figure 1 shows the SEM micrograph of the as-polished cross sections of the coating produced from the $Ti_{41.5}Zr_{41.5}Ni_{17}$ powder according to the parameters given in Table 1. The individual particles are well molten and the coating is well adherent to the substrate (mean bond strength according to EN 582 or equivalent ISO 14916 of 73.5 MPa). The coating porosity is found to be 4.9 vol.% and the hardness is 631.5 HV0.1. Figure 2 shows the XRD of the as-sprayed coating along with the XRDs of the as-cast alloy and the as-received powder. The two primary peaks present belong to the QC phase and it indicates the coating contains a significant amount of the QC i-phase (Ref 24). In addition, an EDS study of the microstructure indicates the presence of Laves phase as well (Ref 25). The as-cast alloy and the as-received powders do not contain any QC phase.

3.2 Coefficient of Friction

The mean of the coefficient of friction (COF) under different sliding velocities and normal loads against

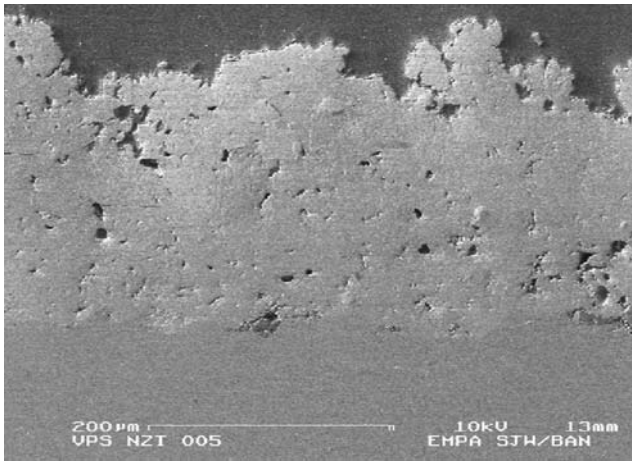

Fig. 1 SEM picture showing the as-polished cross-section of a VPS coating produced from $Ti_{41.5}Zr_{41.5}Ni_{17}$ powders with parameters from Table 1

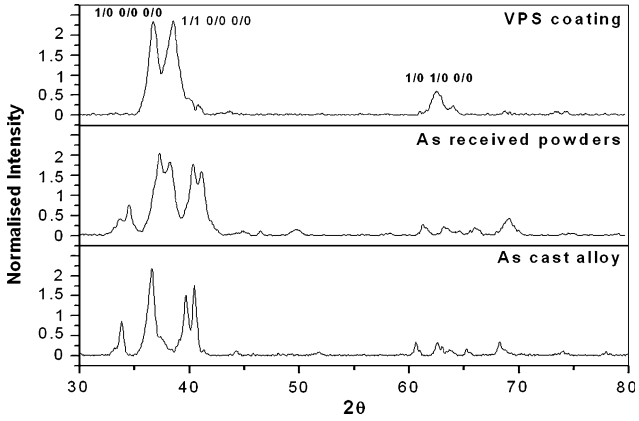

Fig. 2 Combined XRD results of the as-cast alloy, the as-received powder and the as-sprayed coating measured with Mo Kα, but corrected for Cu Kα radiation

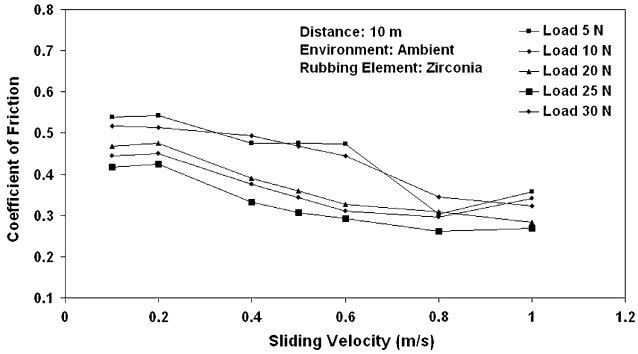

Fig. 3 Variation of coefficient of friction of TiZrNi coatings during sliding against zirconia balls at different normal loads of 5 up to 30 N and sliding velocities of 0.1 up to 1 m/s

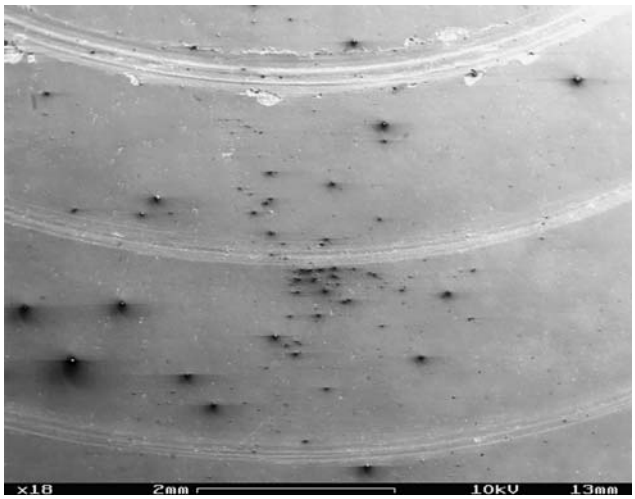

Fig. 4 SE image of three wear tracks of the QC coating created by zirconia balls sliding at a constant sliding velocity of 0.5 m/s and normal loads of 25 N (uppermost track), 10 N (middle track) and 5 N (lowermost track), respectively

zirconia balls are plotted in Fig. 3 for the first 10 m. The coefficient of friction is found to decrease with increase in either sliding velocity or load. Figure 4 is a low magnification secondary electron (SE) image of the coated surface bearing three wear tracks created by zirconia balls sliding at a velocity of 0.5 m/s and normal loads of 25 N (uppermost track), 10 N (middle track) and 5 N (lowermost track), respectively. From this image, it is evident that a higher load brings about considerably higher plastic deformation on the surface. An EDS analysis reveals particles that are broken out fragments of the zirconia balls (Fig. 5, left) and COF in the range of $\mu \approx 0.4$. Rubbing between two hard objects results in a limited amount of plastic deformation of the coating and the fracture of the zirconia ball. The sharp edges of the partly broken zirconia ball causes abrasion of the coating. The unsteady friction coefficient is a result of both the vibration of the instrument in the vertical direction under a low load and a stick-slip phenomenon at the contact region.

Figure 4 shows that in contrast to the lower load scenario (lower track), considerable plastic deformation and side flow occur when the normal load is increased to 25 N (upper track). There is no fractured zirconia particle present on the wear track. Possibly, at this load, the temperature of the contact region is high enough to soften the coating. Low heat conductivities of the QC and zirconia aid the heat retention process (Ref 8, 26). The softened coating yields quickly under the sliding zirconia ball and provides a low friction path to the motion. In other words, at a higher temperature the material softens and its shear strength decreases. Sliding against a material with a reduced shear strength results in lower friction. So the mean coefficient of friction is found to be low at this load. At high sliding velocity, the frictional heat generation at the contact is likely to be high and this results in softening of the coating immediately at the contact point below the zirconia ball.

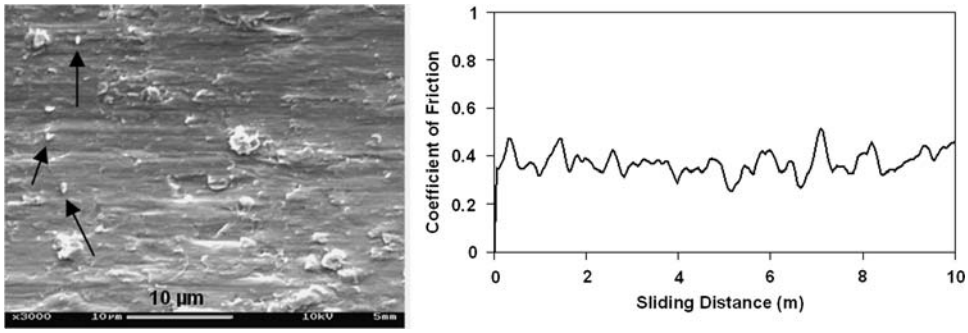

Fig. 5 (*left*) Magnification of middle wear track of Fig. 4 showing the plastic deformation and wear debris from the ZrO_2 ball after the test at 10 N load and 0.5 m/s speed. The arrows show the fractured zirconia particles and (*right*) COF during the first 10 m sliding distance

The low thermal conductivity of both the rubbing elements helps heat retention and severe plastic deformation of the softened coating takes place. The values of the coefficient of friction obtained in this study range between 0.26 and 0.62 with an average of around 0.4. Visual examination of a zirconia ball reveals a clear spot formed by transfer of coating material after running the wear test for about 100 m or so. Undoubtedly, the coating material adheres to zirconia during rubbing. Similar results have been reported by Dubois (Ref 7). It has been observed in these studies that two hard materials in contact lead to formation of small particles by fracture. These particles are picked up from the wear track by the softer member of the rubbing pair and gradually a layer of transferred material forms on it. In fact a clearly visible gray spot has been found to form on the white zirconia balls after sliding. The contact of dissimilar materials is thus transformed to a contact of similar materials and this results in high values of coefficient of friction. In this case, however, the friction experiments have been undertaken for a distance of 10 m only to observe the run-in behavior, where the thickness of the transferred layer formed thereof is likely to be very small. The high friction coefficient observed in this study can thus be partly accounted for by the presence of the thin layer of transferred material mentioned above. A further increase in sliding distance is expected to result in an increase in the thickness of the transferred layer. This in turn will create a situation wherein friction between like materials is encouraged and in such cases even higher values of coefficient of friction is expected, especially in low speed-low load conditions. Also, it can be speculated that the other possible reason for such a value of the coefficient of friction is the presence of crystalline phases in the coating itself (Ref 25).

3.3 Coating Wear

Figure 6 is a record of the mass loss in wear with sliding distance. In the first 50 m of sliding the wear rate is low. During the contact between two hard surfaces, the zirconia ball undergoes fracture and the sharp edges of the fractured zirconia ball and the fractured zirconia particles cause abrasion on the coated surface. Also the metal from the coating is transferred to the zirconia ball and a contact

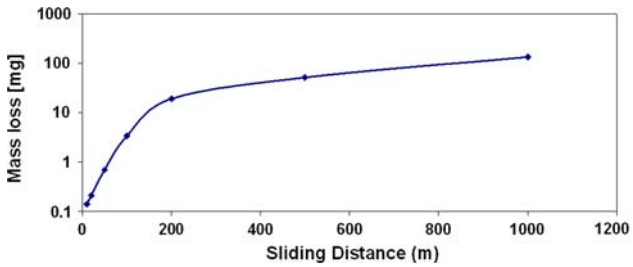

Fig. 6 Mass loss (in logarithmic scale) of the QC coatings during sliding against a zirconia ball as a function of distances; Load 10 N and speed 0.5 m/s

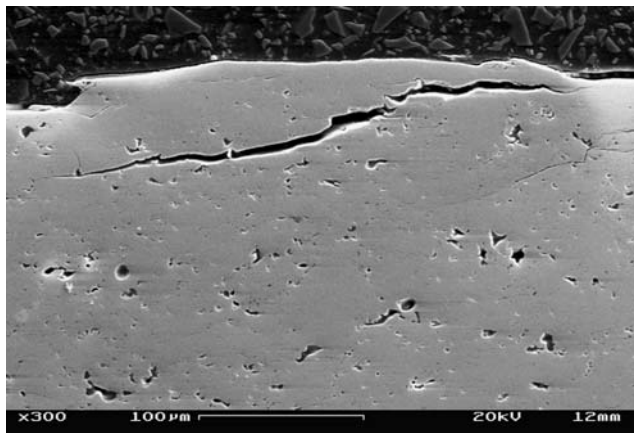

Fig. 7 The SE image (side view) of a worn coating after sliding against a zirconia ball over a distance of 100 m at a load of 10 N and speed of 0.5 m/s

between like materials (the metallic coating and the transferred layer of the coating on the zirconia surface) is established. The mechanism of wear from this point onwards is adhesive. Beyond 100 m, the wear rate increases again and delamination comes into play (Fig. 7). Subsurface cracks grow during the tribo-action of the zirconia ball on the coating surface. This crack growth is encouraged by two factors; the high defect density of thermally sprayed coatings and the inherent brittleness of the QCs. When the crack finally reaches the surface the

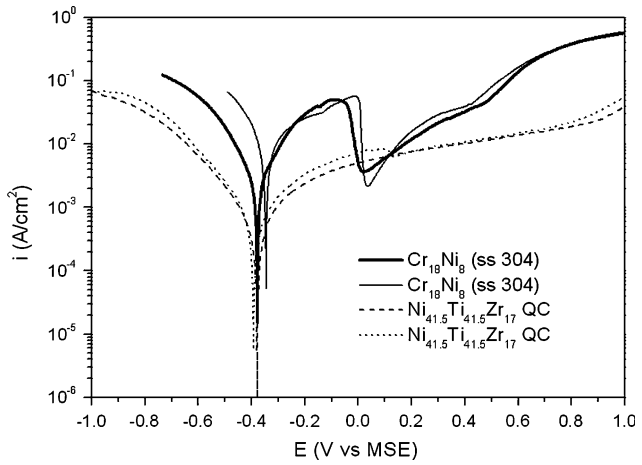

Fig. 8 Logarithmic representation of the polarization curves of the QC coating and the stainless steel in 0.5 M HCl + 0.5 M NaCl (Ref 25)

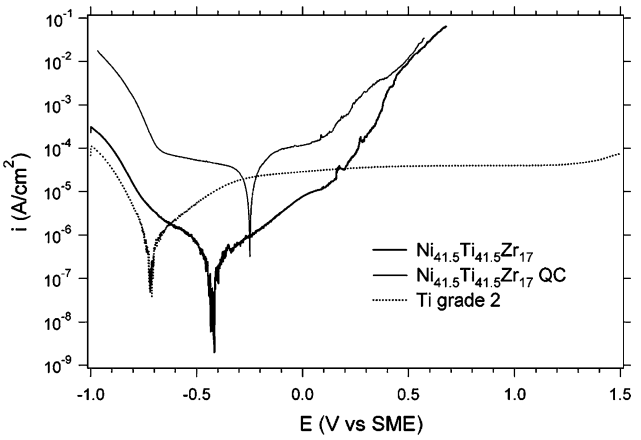

Fig. 9 Logarithmic representation of the polarization curve of the QC coating, the polycrystalline samples of same composition and pure titanium (grade 2) in 1 M HCl. The potential is corrected for the ohmic drop (Ref 25)

Table 3 Immersion corrosion results

Sample type	No.	Mass loss, mg
304 stainless steel	1	3.17
	2	3.51
$Ti_{41.5}Zr_{41.5}Ni_{17}$ coating	1	0.28
	2	1.14
	3	0.86
	4	0.12

delamination of a coating flake occurs. This explains a sudden growth of the wear rate of the coating.

3.4 Corrosion

Table 3 shows the results of the immersion corrosion experiments. The mass loss of stainless steel is consistently above 3 mg, whereas the maximum mass loss for the coating material under identical conditions is 1.14 mg. Clearly the QC alloy offers much higher corrosion resistance than stainless steel under the given conditions. A possible explanation for a high scatter in the mass loss data of the coating is the presence of localized pores. These are usually present in thin thermally sprayed coatings. It is possible that the corrosive media has percolated through one such isolated pore and has attacked the steel substrate underneath, which is much less corrosion resistant.

Logarithmic representations of the measured polarization curves of the QC coating and of 304 stainless steel in 0.5 M HCl + 0.5 M NaCl are given in Fig. 8. This environment with the high chloride concentration is known to favor pitting corrosion, which is a local type of corrosion typically occurring on metals protected by a passivating oxide.

Figure 8 shows that the corrosion potentials E_{corr} of both materials are very similar, but that the corrosion current at E_{corr}, i_{corr}, is much higher for 304 stainless steel than for the QC coating. The stainless steel shows passivation at potentials above 0 V. It remains passive till the onset of pitting corrosion at potentials above approximately 0.5 V. The QC coating is passive over the measured range of potentials till the onset of pitting at about 0.85 V. After experiments, QC as well as 304 samples clearly showed corrosion pits. However, the measured current for the QC samples was up to a magnitude lower than for 304 stainless steel, which is in agreement with the better corrosion behavior in immersion tests. In Fig. 9, polarization curves of the QC coating, a polycrystalline $Ti_{41.5}Zr_{41.5}Ni_{17}$, and titanium in 1 M HCl are given. It is interesting to note that around the corrosion potential E_{corr}, polycrystalline $Ti_{41.5}Zr_{41.5}Ni_{17}$ shows even lower anodic currents than titanium, which is very corrosion resistant due to its dense, protecting, oxide layer. However, at more anodic potentials, polycrystalline $Ti_{41.5}Zr_{41.5}Ni_{17}$ is susceptible to pitting corrosion, whereas titanium is not attacked yet (Fig. 9).

The increase in current for titanium at the anodic end of the measurement is due to the onset of water decomposition in the electrolyte, not to pitting corrosion. By comparing the QC to the polycrystalline material, higher currents for the QC over the whole range of potentials are found. While both materials are passive at E_{corr}, the oxide of the QC seems to be less protective than that of the polycrystalline material, leading to a larger volume of dissolved material. In the case of the polarization curve of the quasicrystalline alloy there exists a well-defined plateau region around the E_{corr} (Fig. 9). In the case of the polycrystalline alloy this plateau region is also present at the corresponding potentials. However, it looks less like a plateau owing to the nature of the logarithmic representation of the curve in the lower current regime, wherein even a small increase in current is detected.

By comparing UBM micrographs of the corroded surfaces, however, the QC phase seems to play a very important role in the corrosion mechanism. The QC surface (Fig. 10, upper) contains a large number of small pits over the whole surface, resulting in a larger loss of

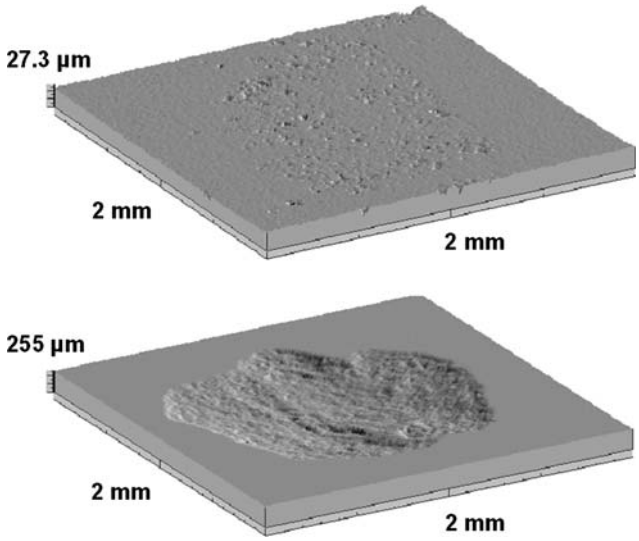

Fig. 10 Surface topography measurements done by scanning laser profilometry of pitted surface of QC (*top*) $Ti_{41.5}Zr_{41.5}Ni_{17}$ and polycrystalline coating (*bottom*) after the linear sweep polarization experiment

material as seen by the higher currents measured during polarization curves. The polycrystalline surface (Fig. 10, lower) reveals fewer but much larger pits, with an almost intact surface in-between pits. A local attack is clearly more dangerous with respect to mechanical failure of a device. The combination of polarization curves and surface topography is in this case important to understand the prevailing corrosion mechanism. In spite of the identical chemical composition, both materials show different corrosion behaviors in chloride environment, which must clearly be due to the differences in their microstructure. It may further be noted that the QC coating like any other plasma sprayed coating contains some pores (typically less than 4%). All other materials (stainless steel, Titanium, Polycrystalline NZT) are bulk materials, either cast or forged.

4. Conclusions

1. At the low velocity regime, i.e., up to 0.2 m/s, motion of the ZrO_2 ball against the coated surface is of ''stick-slip'' nature. The plastic deformation involved is limited. The friction force shows periodic growth and decay. It is speculated that the temperature of the contact is low enough for the QC coating to retain its hardness. The ZrO_2 ball undergoes fracture owing to the contact with the hard QC coating and the COF is high.
2. As the velocity is raised to 0.4 m/s and beyond, the rise in contact temperature apparently is high enough to soften the QC coating and makes it plastically deformable under the contact pressure. The low thermal conductivity of the QC helps in the retention of the high temperature and the resulting softness of the coating. The softened QC layer provides a low friction path to sliding.
3. The friction and wear scenario at a low load (<10 N) is somewhat similar to that in the low velocity regime. Plastic deformation of the coating is limited, fractured ZrO_2 particles are abundant, mean COF is high and the instantaneous coefficient of friction shows large variations. These can be attributed to the expected low contact temperature and the resulting high hardness of the coating undergoing rubbing against zirconia.
4. It is speculated that, as the normal load reaches 20 N, the contact temperature is high enough to soften the top layer of the coating, which in turn provides a low friction path.
5. During rubbing a thin layer of the coating material is transferred to the counterpart transforming the contact to a self-mated type and this is likely to raise the value of COF for the pair of materials considered in this study.
6. QC and polycrystalline coatings show a very different corrosion behavior in chloride environment, which must clearly be due to the differences in their microstructure.

References

1. D. Shechtman, I. Blech, D. Gratias, and J.W. Cahn, Metallic Phase with Long-Range Orientational Order and No Translational Symmetry, *Phys. Rev. Lett.*, 1984, **53**, p 1951-1953
2. Y. Massiani, J.-M. Dubois, S.A. Yaazza, and J.-P. Crousier, Electrochemical Corrosion Behavior of Quasi-Crystalline Coatings Prepared by Plasma Torch, *Matériaux Tech.*, 1996, **84**, p 39-45
3. T. Klein and O.G. Symko, Formation of AlCuFe Quasicrystalline Thin Films by Solid State Diffusion, *Appl. Phys. Lett.*, 1994, **64**(4), p 431
4. J.M. Dubois, S.S. Kang, and S. von Stebut, Quasicristalline Low-Friction Coatings, *J. Mater. Sci. Lett.*, 1991, **10**, p 537-541
5. C.J. Jenks and P.A. Theil, Surface Properties of Quasicrystals, *MRS Bull*, 1997, **22**(11), p 55
6. F. Cyrot-Lackmann, Quasicrystals as Potential Candidates for Thermoelectric Materials, *Mater. Sci. Eng. A*, 2000, **294-296**, p 611-612
7. J.-M. Dubois, New Prospects from Potential Applications of Quasicrystalline Materials, *Mater. Sci. Eng. A*, 2000, **294-296**, p 4-9
8. D.J. Sordelet, S.D. Widener, Y. Tang, and M.F. Besser, Characterization of a Commercially Produced Al-Cu-Fe-Cr Quasicrystalline Coating, *Mater. Sci. Eng. A*, 2000, **294-296**, p 834-837
9. J.M. Dubois, S.S. Kang, and A. Perrot, Towards Applications of Quasicrystals, *Mater. Sci. Eng. A*, 1994, **179-180**, p 122
10. D.J. Sordelet, M.F. Besser, and I.E. Anderson, Particle Size Effects on Chemistry and Structure of Al-Cu-Fe Quasicrystalline Coatings, *J. Therm. Spr. Techn.*, 1996, **5**, p 161-174
11. J.P. Davis, E.H. Majzoub, J.M. Simmons, and K.F. Kelton, Ternary Phase Diagram Studies in Ti-Zr-Ni Alloys, *Mater. Sci. Eng. A*, 2000, **294-296**, p 104-107
12. P.A. Thiel, A.I. Goldman, and C.J. Jenks, Physical Properties of Quasicrystals. Springer Series in Solid State Science, Vol. 126, Z.M. Stadnik, Ed., Berlin, Germany: Springer-Verlag, 1999, p 327
13. K.F. Kelton, W.J. Kim, and R.M. Stroud, A Stable Ti-based Quasicrystal, *Appl. Phys. Lett.*, 1997, **70**, p 3230-3232
14. Y. Massiani, S. Ait Yaazza, J.P. Crousier, and J.M. Dubois, Electrochemical Behaviour of Quasicrystalline Alloys in Corrosive Solutions, *J. Non-Cryst. Solids*, 1993, **159**, p 92

15. P.C. Gibbons and K.F. Kelton, Physical Properties of Quasicrystals. Springer Series in Solid State Science, Vol. 126, Z.M. Stadnik, Ed., Berlin, Germany: Springer-Verlag, 1999, p 403
16. J.M. Dubois, S.S. Kang, and Y. Massiani, Application of Quasicrystalline Alloys to Surface Coating of Soft Metals, *J. Non-Cryst. Solids*, 1993, **153**, p 443
17. C.J. Jenks, P.J. Pinhero, S.L. Chang, J.W. Andregg, M.F. Besser, D.J. Sordelet, and P.A. Theil, *New Horizons in Quasicrystals*, A.I. Goldman, D.J. Sordelet, P.A. Theil, and J.M. Dubois, Ed., World Scientific, 1997, p 157
18. F.J. Hermanek, Processing Quasicrystalline Powders to Produce Variable and Unique Coating Properties, *Thermal Spray: Surface Engineering via Applied Research*, Vol 1, C.C. Berndt, Ed., May 8-11, 2000 (Montréal, Québec, CA), ASM International, 2000, p 567-573
19. E. Lugscheider, C. Herbst-Dederichs, and A. Reimann, Thermally Sprayed Quasicrystal Composite Coatings for Bearings and Other Friction Threaded Applications, *Thermal Spray: Surface Engineering via Applied Research*, Vol 1, C.C. Berndt, Ed., May 8-11, 2000 (Montréal, Québec, CA), ASM International, 2000, p 843–849
20. A. Reimann and E. Lugscheider, HVOF-Sprayed Quasi-crystal Composite Coatings for Bearing Applications, *Thermal Spray 2001: New Surfaces for a New Millennium*, C.C. Berndt, K.A. Khor, and E.F. Lugscheider, Ed., May 28-30, 2001 (Singapore), ASM International, 2001, p 33-39
21. D.J. Sordelet, P.D. Krotz, R.L. Daniel, Jr., and M.F. Smith, Microstructure and Wear Behavior of Quasicrystalline Thermal Sprayed Coatings, *Thermal Spraying: Current Status and Future Trends*, Akira Ohmori, Ed., May 22-26, 1995 (Kobe, Japan), High Temperature Society of Japan, 1995, p 627-632
22. J.E. Shield, A.I. Goldman, I.E. Anderson, T.W. Ellis, R.W. McCallum, and D.J. Sordellet, US Patent # 5,433,978, 1993
23. D.J. Sordelet, M.F. Besser, and J. L. Logsdon, Abrasive Wear Behavior of Al-Cu-Fe Quasicrystalline Composite Coatings, *Mater. Sci. Eng. A*, 1998, **255**, p 54-65
24. E.H. Majzoub, ''Ti Based Icosahedral Quasicrystals and Approximants: Phase Formation, Cluster Structure and Hydrogenation,'' Ph.D. Thesis, Washington Uni., 2000
25. P.P. Bandyopadhyay, P. Kern, and S. Siegmann, Corrosion behavior of vacuum plasma sprayed Ti-Zr-Ni quasicrystal coatings, *J. Mater. Sci.*, 2004, **39**, p 6101-6104
26. J. Pezdirnik, J. Vizintin, and B. Podgornik, Temperatures at the interface and inside an oscillatory sliding microcontact—theoretical part, *Tribol. Int.*, 1999, **32**, p 481-489